

Low two-level-system noise in hydrogenated amorphous silicon

Fabien Defrance,¹ Andrew D. Beyer,¹ Jordan Wheeler,² Jack Sayers,³ and Sunil R. Golwala³

¹*Jet Propulsion Laboratory, California Institute of Technology, Pasadena, CA 91109, USA*

²*National Institute of Standards and Technology, Boulder, CO 80305, USA*

³*California Institute of Technology, Pasadena, CA 91125, USA*

(*fabien.m.defrance@jpl.nasa.gov)

(Dated: 16 December 2024)

At sub-Kelvin temperatures, two-level systems (TLS) present in amorphous dielectrics source a permittivity noise, degrading the performance of a wide range of devices using superconductive resonators such as qubits or kinetic inductance detectors. We report here on measurements of TLS noise in hydrogenated amorphous silicon (a-Si:H) films deposited by plasma-enhanced chemical vapor deposition (PECVD) in superconductive lumped-element resonators using parallel-plate capacitors (PPCs). The TLS noise results presented in this article for two recipes of a-Si:H improve on the best achieved in the literature by a factor >5 for a-Si:H and other amorphous dielectrics and are comparable to those observed for resonators deposited on crystalline dielectrics.

©2024. All rights reserved.

Superconductive devices like kinetic inductance detectors (KIDs) and superconductive qubits exhibit an excess frequency noise and loss at low temperatures (below a few Kelvins) that was shown¹⁻³ to originate from two-level systems (TLS)^{4,5}. The standard tunneling model (STM) describes TLS as defects that can switch between two different configurations^{4,6}. Such TLS can also change state by phonon emission, introducing a loss mechanism that, via the fluctuation-dissipation theorem⁷, results in noise in dielectric permittivity and thus, in resonators, resonant frequency^{1-3,8,9}. Because the atomic scale disorder giving rise to TLS in amorphous dielectrics is vastly reduced in crystalline dielectrics, they are preferentially selected as substrates for superconductive devices where low loss and low noise are critical, though it should be noted that unavoidable surface oxides still host TLS³. However, fabricating multi-layer structures with crystalline dielectrics remains extremely challenging^{10,11}, constraining such devices to single-layer architectures on crystalline substrates. For KIDs, which now primarily use single-layer interdigitated capacitors (IDCs), such a limitation leads to undesirable detector characteristics such as sensitivity to light unintentionally routed by the optically inactive capacitor to the inductor¹² and/or a large capacitor footprint. Parallel-plate capacitors (PPCs) enabled by amorphous dielectrics would eliminate these properties. However, literature measurements of superconductive resonators using amorphous dielectrics^{9,13-15} show TLS noise levels more than 100 times larger than observed on crystalline substrates. In this article, we report on superconductive resonators using PPCs that incorporate hydrogenated amorphous silicon (a-Si:H) with extremely low TLS noise, comparable to that of resonators fabricated on crystalline silicon and sapphire. Because it is easily depositable, this novel a-Si:H opens the door to development of low-noise superconductive devices with multi-layer architectures.

As expected from the fluctuation-dissipation theorem, TLS are observed to contribute loss at low temperature, limiting the quality factor of superconductive resonators, the transmis-

sion of microstriplines, and the coherence of qubits^{3,14,16-22}. We have shown in a previous article²³ that our a-Si:H recipes have a radio-frequency (RF) loss tangent at 0 K and low stored power of 7×10^{-6} , which is the lowest published loss tangent for amorphous dielectrics and approaches that of crystalline silicon²⁴. The TLS noise results we present here were obtained with the same a-Si:H recipes and the same devices as those loss results. All the fabrication details for the a-Si:H recipes can be found there.

Each device comprises a 50 Ω coplanar waveguide (CPW) readout feedline inductively coupled to six lumped element LC resonators. These LC resonators, made with Niobium (Nb), are composed of an inductor and two PPCs in series, with a 800 nm layer of a-Si:H as the capacitor dielectric. The resonance frequencies of the six resonators are grouped into two triplets centered on 0.84 GHz and 1.55 GHz, and, within each triplet, the designed resonance frequencies are in the ratio 1:1.05:1.10. Two different a-Si:H recipes (designated with the letters A and B) were used to fabricate these devices. For each recipe, one wafer with 4 devices was fabricated, with the devices from a given wafer designated with a number from 1 to 4. The fabrication was carried out at the Caltech Kavli Nanoscience Institute (KNI) clean room using PECVD for recipe A and at the NASA Jet Propulsion Laboratory's MicroDevices Laboratory (MDL) using inductively coupled plasma (ICP) PECVD for recipe B.

Two TLS noise measurement campaigns were conducted. At Caltech, we measured the TLS noise as a function of feedline readout power for five devices at a base temperature of 230 mK. At NIST (National Institute of Standards and Technology), using a dilution fridge able to reach temperatures as low as 20 mK, we measured the TLS noise as a function of power and temperature for two of the five devices initially measured at Caltech.

Caltech's experimental setup is the same as described previously²³ except that we replaced the VNA (vector network analyzer) by the readout system developed by Minutolo et al.²⁵ using a USRP X300 (universal software radio peripheral)

instrument with UBX-160 daughterboard, commercialized by the company Ettus²⁶. Unlike a VNA, this system records the on-resonance network transmission time-stream, which we use to measure its noise power spectral density. The system’s 160 MHz RF bandwidth, centered on a local oscillator whose frequency can be set between DC and 6 GHz, enables noise PSD measurements for multiple resonators. To measure TLS noise at different resonator stored powers/energies while maintaining constant USRP output and input power levels and thus signal-to-noise ratio, room-temperature variable attenuators before and after the cryostat are used: the feedline readout power at the device is swept by changing the value of the input attenuator, and the output attenuator is varied by a cancelling amount.

The NIST setup instead uses a standard homodyne IQ mixing setup. A signal generator emits a tone at f_{res} that is routed to the device, amplified by a cryogenic low-noise high electron mobility transistor (HEMT) amplifier, and mixed with the original signal by a TSC AD0540 IQ mixer, as described previously¹. An analog-to-digital converter (ADC) digitizes the in-phase and quadrature (I and Q) signals generated by the IQ mixer. As for the Caltech setup, variable attenuators before and after the cryostat ensure that the power levels received by the IQ mixer and the ADC stay constant as the power at the device is varied.

Each noise measurement includes three steps:

1. Resonance fit: we measure the complex transmission as a function of frequency, $S_{21}(f)$, across the resonance. Using the python package SCRAPS²⁷, we fit $S_{21}(f)$ and extract the resonance frequency f_{res} , the internal quality factor Q_i , and coupling quality factor Q_c .
2. Calibration: $S_{21}(f)$ is measured for two tones a few tens of kHz below and above f_{res} (B_1 and B_2 in Figure 1). The direction $\vec{B_1B_2}$ corresponds to the frequency direction (tangent to the resonance circle), while the distance $|B_1B_2|$, in volts, provides the volts-to-fractional-frequency conversion coefficient $\zeta = \Delta f / (|B_1B_2| \times f_{res})$, with Δf the frequency difference between B_1 and B_2 .
3. Noise measurement: time-streams of 60 seconds are recorded.

The Caltech USRP setup provided noise time-streams sampled at 2 MHz, while the NIST setup provided time-streams sampled at 2.5 MHz, both after appropriate anti-alias filtering. The cable delay, obtained from the resonance fit, is removed. Using the frequency direction determination and the conversion coefficient ζ from the calibration dataset, the noise time-streams are rotated to the frequency-dissipation basis and the frequency-direction time-stream converted to fractional-frequency units. Fractional-frequency noise PSDs are then calculated. They consist primarily of white noise and TLS noise, as shown in Figure 2.

To measure the TLS noise as a function of stored power, devices A(1), A(2), B(1), B(2), and B(3) were tested in the Caltech setup at 230 mK. Across these five devices, a total

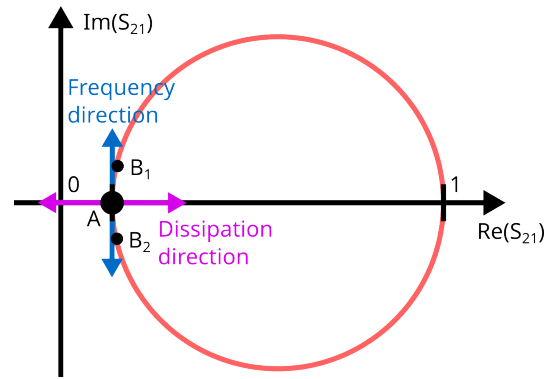


FIG. 1. After removal of the cable delay component, the complex transmission of the resonator as a function of frequency, $S_{21}(f)$, follows the red circle (also called the “resonance circle” or “IQ circle”). The orientation displayed may require removal of rotations of the circle about the complex origin and/or about its own center²⁸. The point A on the circle, located at f_{res} , represents the location of the noise measurement. The two points B_1 and B_2 , on each side of A, show the calibration measurements that identify the frequency-dissipation basis.

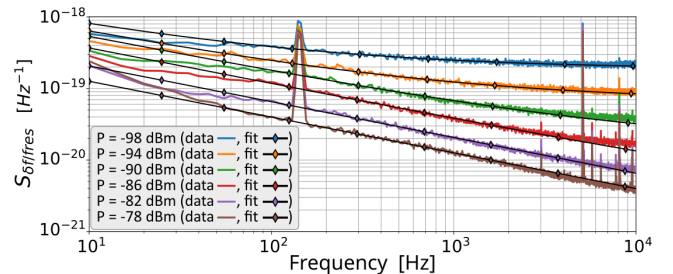


FIG. 2. Fractional-frequency noise PSD ($S_{\delta f/f_{res}}$) of 847 MHz resonance on device B(2) as a function of audio frequency ν . The feedline readout power at the device was swept between -98 dBm and -78 dBm, corresponding to about $200 - 2000$ V/m in electric field and $3 \times 10^6 - 3 \times 10^8$ in photon number. $S_{\delta f/f_{res}}$ can be fit well by a sum of TLS and white noise, $a \times \nu^{-0.5} + b$.

of 18 resonances were measured at a range of feedline readout powers, approximately -100 dBm to -75 dBm (at the device). The fractional-frequency noise PSD measurements and corresponding fits for the 847 MHz resonance on device B(2) are presented in Figure 2. These measurements, conducted at multiple feedline readout powers, illustrate the characteristic TLS noise behavior observed for most resonances. The main parasitic spectral lines seen in Figure 2 come from the cryostat’s pulse-tube cooler valve motor. Because these spectral lines did not impact the measurements or fitting, we did not shut off the pulse-tube cooler to eliminate them. The measured frequency noise PSDs are very reproducible above 100 Hz audio frequency, but, at lower frequencies, they tend to vary slightly between datasets and cooldowns and are thus less reliable. We have therefore restricted the fitting of a noise model to the range 200 Hz to 2 kHz. The model consists of the sum of a TLS and a white noise term, $a \times \nu^\alpha + b$, where ν is the audio frequency.

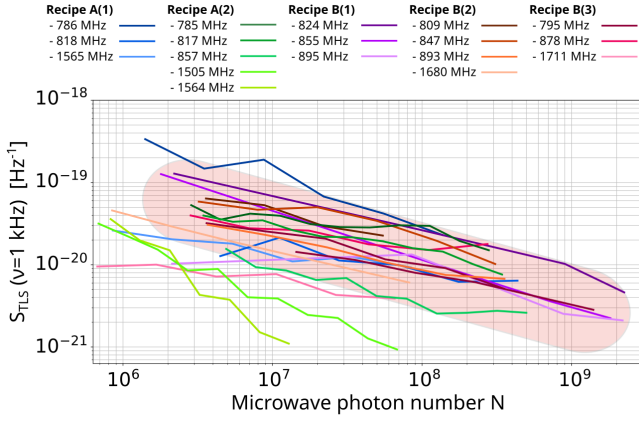


FIG. 3. TLS fractional-frequency noise PSD measured at 1 kHz as a function of stored microwave energy measured in photon units for 18 resonators across five devices fabricated using recipes A and B.

Previous studies^{1,2,14,29–31} show that the TLS noise PSD, S_{TLS} , scales as $T^{-\beta}$, $P_{\text{res}}^{-0.5}$, and ν^α with T the resonator temperature, P_{res} the stored power in the resonator, and ν the audio frequency. For $T > 100$ mK, literature values of β are: 2^{13} , 1.73^{32} , $1.3 - 1.65^{33}$, $1.2 - 1.4^{30}$, $\approx 0.79^{15}$, and $0.55 - 1.35^{14}$ (estimated graphically from Figure 11). The large range of β can be explained by its power dependence. Gao et al.¹³ (Figure 5.21) and Kouwenhoven et al.¹⁴ show that β decreases with increasing stored power, suggesting that partial saturation of TLSs by stored power reduces the temperature dependence of TLS noise. With regard to the ν dependence, while most TLS noise measurements using homodyne setups find values of α close to $-0.5^{1,2,15,31}$, measurements from Burnett et al.^{29,30} using a Pound locking loop seem to indicate that, at frequencies below about 10 Hz, the logarithmic slope of S_{TLS} is $\alpha = -1$, as expected for flicker frequency noise, but they did not measure α above 100 Hz. Recently, Kouwenhoven et al.¹⁴ were able to measure S_{TLS} between 1 Hz and 10 kHz. They found $\alpha \approx -1$ below 100 Hz and $\alpha \approx -0.5$ above 100 Hz – 1 kHz, with a smooth transition between slopes, which reconciles all previous α results. They also show that the $\nu^{-0.5}$ and ν^{-1} model components follow the usual TLS power and temperature dependences. We note that the presence of both slopes had also been seen by Gao et al. in 2007¹, with a transition around 10 Hz, but, at the time, the $\alpha = -1$ slope had been attributed to readout electronics noise. Our measurements and fits of S_{TLS} between 200 Hz and 2 kHz follow $\alpha \approx -0.5$, in accordance with previous measurements at $\nu > 100$ Hz. Our most reliable fits of α were obtained at high feedline readout powers, where the white noise level is low compared to the TLS noise and the TLS noise slope is clearly visible, as illustrated by Figure 2. To reduce the degeneracy between the fit parameters a , b , and α , and because α is expected to be the same for all resonators, we used the value $\alpha = -0.5$ obtained from the fits at high feedline readout powers as a fixed parameter for all the fits, only varying a and b .

Using the values of a given by the fit, we show in Figure 3 S_{TLS} at $\nu = 1$ kHz as a function of stored microwave energy,

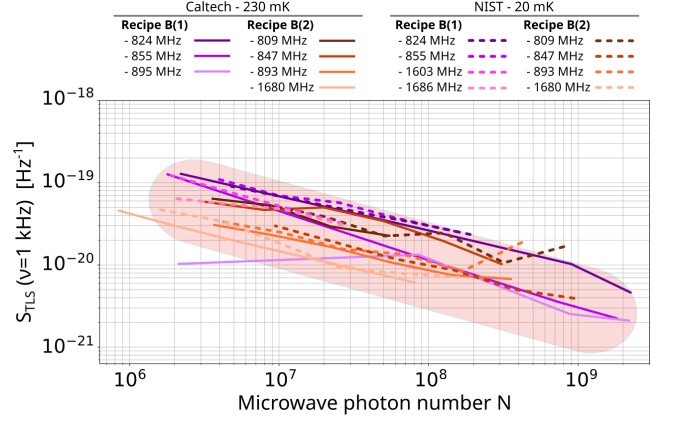


FIG. 4. TLS fractional-frequency noise PSD measured at 1 kHz for devices B(1) and B(2) at Caltech (230 mK) and NIST (20 mK).

expressed in photon number, for all the devices measured at Caltech. For each resonator, we calculated the microwave photon number corresponding to each feedline readout power P_{feed} using:

$$N = \frac{W}{hf_{\text{res}}} = \frac{P_{\text{res}}}{hf_{\text{res}}^2} = \frac{P_{\text{feed}} Q_r^2}{\pi h f_{\text{res}}^2 Q_c} \quad (1)$$

where P_{res} is the stored power in the resonator and h is Planck's constant. The provenance of Equation 1 and the correspondence to electric field are available elsewhere²³. We see some variation among the 18 curves shown in Figure 3, even for resonators incorporating the same a-Si:H film on the same device. Multiple measurements were taken for each resonator and they are reproducible, suggesting that the variations may arise from film non-uniformity or defects leading to TLS density variations. Figure 3 shows no obvious difference in S_{TLS} between recipes A and B. The 1 decade variation in S_{TLS} in Figure 3 combined with the modest factor of ≈ 2 difference in loss tangent between the recipes would, however, hide all but very strong dependences of noise level on loss tangent. To give a sense of the range of a-Si:H TLS noise level for our recipes, we define in Figure 3 a red envelope inside of which most of the S_{TLS} vs. N reside, leaving out only three outlier datasets.

To check the results obtained at Caltech, we re-tested devices B(1) and B(2) at NIST three years later. The TLS fractional-frequency noise PSDs at $\nu = 1$ kHz measured at NIST at 20 mK are plotted in Figure 4, overlaid with Caltech measurements obtained for the same devices at 230 mK. For device B(1), not all resonances gave reliable TLS noise measurements with both systems. The Caltech data for the 1603 MHz and 1680 MHz resonances displayed white noise well above the expected TLS noise level. The NIST data for the 895 MHz resonance evidenced a strong additional noise that rose steeply with decreasing audio frequency. Comparing the six remaining resonances common to the Caltech and NIST datasets, we observe less than a factor 2 difference.

While the consistency between datasets is encouraging, we would have expected the NIST measurements to be higher

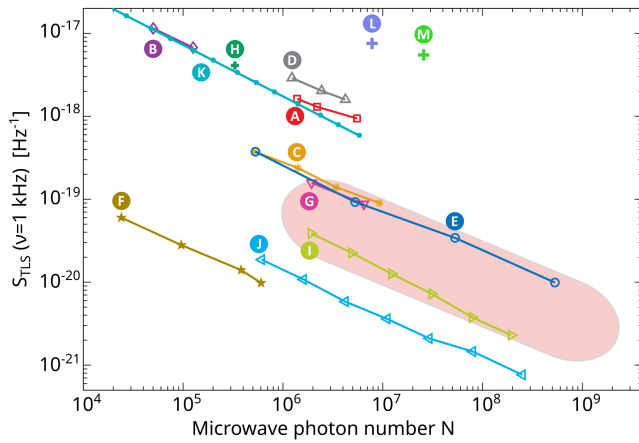


FIG. 5. TLS fractional-frequency noise PSD measured at 1 kHz as a function of stored microwave energy measured in photon units for a variety of resonators. (A) Al on Si, $f_{res}=5.8$ GHz, $T=120$ mK¹; (B) Al on Si CPW, 4.8 GHz, 120 mK¹; (C) Al on sapphire CPW, 4 GHz, 120 mK¹; (D) Al on Ge CPW, 8 GHz, 120 mK¹; (E) Nb on Si CPW, 5.1 GHz, 120 mK¹; (F) Nb IDC on Si with Al CPW inductor, 5.6 GHz, 120 mK⁸; (G) TiN on Si CPW, 6 GHz, 100 mK³⁴; (H) Al-a-Si:H-Al microstrip, 9 GHz, 150 mK; (I) NbTiN on Si CPW, 4.4 GHz, 310 mK³⁵; (J) NbTiN on Si CPW, 2.64 GHz, 310 mK³⁵; (K) NbTiN-a-Si:C-NbTiN PPC, 5.15 GHz, 100 mK¹⁴; (L) Al-SiN_x-Al PPC, 1.9 GHz, 100 mK¹⁵; (M) Al-Si₃N₄-Al PPC, 2.2 GHz, 100 mK¹⁵. **(Red envelope) Nb-a-Si:H-Nb PPC, 800 MHz and 1.6 GHz, 20 mK and 230 mK.** Adapted with permission from J. Zmuidzinas⁹. Copyright 2012, Annual Reviews.

than the Caltech data due to the temperature dependence of TLS noise. In data taken at NIST not presented here, we found consistency with the literature temperature dependence reviewed earlier, with values of β varying from 0.4 to 1.3 over the stored powers probed. For $N \lesssim 10^8$, these dependences imply an expected factor of 1.5 – 2 difference between the NIST and Caltech datasets. The most likely explanation for this apparent discrepancy is a systematic error in the feedline readout power and thus the microwave photon number: the feedline readout power at the device is only known to an accuracy of 2 – 3 dBm.

In order to compare our a-Si:H TLS noise results with the literature, we overlaid the envelope of our measurements on Figure 14 of the review paper by Zmuidzinas⁹, reproduced in Figure 5 and augmented with recent results on other amorphous dielectrics (K, L, and M). The K data were reported at $\nu = 10$ Hz, so we used their measurement of $\alpha \approx -1$ to extrapolate to $\nu = 1$ kHz¹⁴. We see that the $S_{TLS}(\nu = 1$ kHz) results presented in this article are 8 – 80 times lower than previous measurements for a-Si:H (H), 5 – 50 times lower than for hydrogenated amorphous silicon carbide (a-SiC:H; (K)), >100 times lower than for silicon nitride (SiN_x (L) & Si₃N₄ (M)), and comparable to the TLS noise level usually achieved on crystalline substrates such as silicon (A, B, E, F, G, I, J) and sapphire (C).

We conclude by noting that the competitive level of TLS noise provided by the two a-Si:H recipes reported here renders PPC-based architectures for superconductive resonators

a viable alternative to those using CPWs or IDCs. As noted earlier, such an architecture could be transformative for KIDs, vastly reducing their footprint and capacitor-routed direct optical absorption. We are actively applying these a-Si:H PPCs in KIDs for mm/submm astronomy for continuum imaging (the NEW-MUSIC³⁶ instrument for the Leighton Chajnantor Telescope) and filterbank spectroscopy³⁷.

ACKNOWLEDGMENTS

This work has been supported by the JPL Research and Technology Development Fund, the National Aeronautics and Space Administration under awards 80NSSC18K0385 and 80NSSC22K1556, and the Department of Energy Office of High-Energy Physics Advanced Detector Research program under award DOE-SC0018126. A. B. and F. D. carried out research/fabrication at the Jet Propulsion Laboratory, operated by the California Institute of Technology under a contract with the National Aeronautics and Space Administration (80NM0018D0004). The authors would like to thank J. Gao for his very helpful comments, D. Cunnane for early discussions of a-Si:H fabrication techniques, P. Day for early measurements of a-Si:H PPC TLS noise, and M. Hollister for design and construction of the cryostat used for this work.

- ¹J. Gao, J. Zmuidzinas, B. A. Mazin, H. G. LeDuc, and P. K. Day, “Noise properties of superconducting coplanar waveguide microwave resonators,” *Applied Physics Letters* **90**, 102507 (2007), <https://doi.org/10.1063/1.2711770>.
- ²J. Gao, M. Daal, J. M. Martinis, A. Vayonakis, J. Zmuidzinas, B. Sadoulet, B. A. Mazin, P. K. Day, and H. G. LeDuc, “A semiempirical model for two-level system noise in superconducting microresonators,” *Applied Physics Letters* **92**, 212504 (2008), <https://doi.org/10.1063/1.2937855>.
- ³J. Gao, M. Daal, A. Vayonakis, S. Kumar, J. Zmuidzinas, B. Sadoulet, B. A. Mazin, P. K. Day, and H. G. LeDuc, “Experimental evidence for a surface distribution of two-level systems in superconducting lithographed microwave resonators,” *Applied Physics Letters* **92**, 152505 (2008), <https://doi.org/10.1063/1.2906373>.
- ⁴W. A. Phillips, “Two-level states in glasses,” *Reports on Progress in Physics* **50**, 1657–1708 (1987).
- ⁵P. Esquinazi, ed., “Tunneling systems in amorphous and crystalline solids,” (Springer Berlin Heidelberg, Berlin, Heidelberg, 1998).
- ⁶C. Müller, J. H. Cole, and J. Lisenfeld, “Towards understanding two-level systems in amorphous solids: insights from quantum circuits,” *Reports on Progress in Physics* **82**, 124501 (2019).
- ⁷H. B. Callen and T. A. Welton, “Irreversibility and Generalized Noise,” *Physical Review* **83**, 34–40 (1951).
- ⁸O. Noroozian, J. Gao, J. Zmuidzinas, H. G. LeDuc, and B. A. Mazin, “Two-level system noise reduction for microwave kinetic inductance detectors,” *AIP Conference Proceedings* **1185**, 148–151 (2009), <https://aip.scitation.org/doi/pdf/10.1063/1.3292302>.
- ⁹J. Zmuidzinas, “Superconducting microresonators: Physics and applications,” *Annual Review of Condensed Matter Physics* **3**, 169–214 (2012), <https://doi.org/10.1146/annurev-conmatphys-020911-125022>.
- ¹⁰K. L. Denis, N. T. Cao, D. T. Chuss, J. Eimer, J. R. Hinderks, W. Hsieh, S. H. Moseley, T. R. Stevenson, D. J. Talley, K. U.-yen, and E. J. Wollack, “Fabrication of an antenna-coupled bolometer for cosmic microwave background polarimetry,” *AIP Conference Proceedings* **1185**, 371–374 (2009), <https://aip.scitation.org/doi/pdf/10.1063/1.3292355>.
- ¹¹A. D. Beyer, M. I. Hollister, J. Sayers, C. F. Frez, P. K. Day, and S. R. Golwala, “Fabricating with crystalline si to improve superconducting detector performance,” *Journal of Physics: Conference Series* **834**, 012006 (2017).
- ¹²S. R. Golwala, C. Bockstiegel, S. Brugger, N. G. Czakon, P. K. Day, T. P. Downes, R. Duan, J. Gao, A. K. Gill, J. Glenn, M. I. Hollister, H. G. LeDuc,

- P. R. Maloney, B. A. Mazin, S. G. McHugh, D. Miller, O. Noroozian, H. T. Nguyen, J. Sayers, J. A. Schlaerth, S. Siegel, A. K. Vayonakis, P. R. Wilson, and J. Zmuidzinas, "Status of music, the multiwavelength sub/millimeter inductance camera," *Proc.SPIE* **8452**, 8452 – 8452 – 21 (2012).
- ¹³J. Gao, *The Physics of Superconducting Microwave Resonators*, Ph.D. thesis, California Institute of Technology (2008).
- ¹⁴K. Kouwenhoven, G. van Doorn, B. Buijtdorp, S. de Rooij, D. Lamers, D. Thoen, V. Murugesan, J. Baselmans, and P. de Visser, "Geometry dependence of two-level-system noise and loss in *a*-SiC:H parallel-plate capacitors for superconducting microwave resonators," *Phys. Rev. Appl.* **21**, 044036 (2024).
- ¹⁵J. Sun, S. Shu, Y. Chai, L. Zhu, L. Zhang, Y. Li, Z. Liu, Z. Li, Y. Xu, D. Yan, W. Guo, Y. Wang, and C. Liu, "Cryogenic microwave performance of silicon nitride and amorphous silicon deposited using low-temperature icpcvd," (2024), arXiv:2409.09301 [physics.ins-det].
- ¹⁶J. M. Martinis, K. B. Cooper, R. McDermott, M. Steffen, M. Ansmann, K. D. Osborn, K. Cicak, S. Oh, D. P. Pappas, R. W. Simmonds, and C. C. Yu, "Decoherence in josephson qubits from dielectric loss," *Phys. Rev. Lett.* **95**, 210503 (2005).
- ¹⁷A. D. O'Connell, M. Ansmann, R. C. Bialczak, M. Hofheinz, N. Katz, E. Lucero, C. McKenney, M. Neeley, H. Wang, E. M. Weig, A. N. Cleland, and J. M. Martinis, "Microwave dielectric loss at single photon energies and millikelvin temperatures," *Applied Physics Letters* **92**, 112903 (2008), <https://doi.org/10.1063/1.2898887>.
- ¹⁸B. A. Mazin, D. Sank, S. McHugh, E. A. Lucero, A. Merrill, J. Gao, D. Pappas, D. Moore, and J. Zmuidzinas, "Thin film dielectric microstrip kinetic inductance detectors," *Applied Physics Letters* **96**, 102504 (2010), <https://doi.org/10.1063/1.3314281>.
- ¹⁹A. Bruno, S. T. Skacel, C. Kaiser, S. Wünsch, M. Siegel, A. V. Ustinov, and M. P. Lisitskiy, "Investigation of Dielectric Losses in Hydrogenated Amorphous silicon (*a*-Si:H) thin Films Using Superconducting Microwave Resonators," *Physics Procedia* **36**, 245–249 (2012).
- ²⁰B. T. Buijtdorp, J. Bueno, D. J. Thoen, V. Murugesan, P. M. Sberna, J. J. A. Baselmans, S. Vollebregt, and A. Endo, "Characterization of low-loss hydrogenated amorphous silicon films for superconducting resonators," in *Millimeter, Submillimeter, and Far-Infrared Detectors and Instrumentation for Astronomy X*, Vol. 11453, edited by J. Zmuidzinas and J.-R. Gao, International Society for Optics and Photonics (SPIE, 2020) pp. 459 – 472.
- ²¹S. Hähnle, K. Kouwenhoven, B. T. Buijtdorp, A. Endo, K. Karatsu, D. J. Thoen, V. Murugesan, and J. J. A. Baselmans, "Superconducting Microstrip Losses at Microwave and Submillimeter Wavelengths," *Physical Review Applied* **16**, 014019 (2021).
- ²²B. T. Buijtdorp, S. Vollebregt, K. Karatsu, D. J. Thoen, V. Murugesan, K. Kouwenhoven, S. Hähnle, J. J. A. Baselmans, and A. Endo, "Hydrogenated amorphous silicon carbide: A low-loss deposited dielectric for microwave to submillimeter-wave superconducting circuits," *Phys. Rev. Appl.* **18**, 064003 (2022).
- ²³F. Defrance, A. D. Beyer, S. Shu, J. Sayers, and S. R. Golwala, "Characterization of the low electric field and zero-temperature two-level-system loss in hydrogenated amorphous silicon," *Phys. Rev. Mater.* **8**, 035602 (2024).
- ²⁴S. J. Weber, K. W. Murch, D. H. Slichter, R. Vijay, and I. Siddiqi, "Single crystal silicon capacitors with low microwave loss in the single photon regime," *Applied Physics Letters* **98**, 172510 (2011), <https://doi.org/10.1063/1.3583449>.
- ²⁵L. Minutolo, B. Steinbach, A. Wandui, and R. O'Brient, "A flexible gpu-accelerated radio-frequency readout for superconducting detectors," *IEEE Transactions on Applied Superconductivity* **PP**, 1–1 (2019).
- ²⁶<https://www.ettus.com/>.
- ²⁷F. W. Carter, T. S. Khaire, V. Novosad, and C. L. Chang, "scraps: An open-source python-based analysis package for analyzing and plotting superconducting resonator data," *IEEE Transactions on Applied Superconductivity* **27**, 1–5 (2017).
- ²⁸M. S. Khalil, M. J. A. Stoutimore, F. C. Wellstood, and K. D. Osborn, "An analysis method for asymmetric resonator transmission applied to superconducting devices," *Journal of Applied Physics* **111**, 054510-054510-6 (2012), arXiv:1108.3117 [cond-mat.supr-con].
- ²⁹J. Burnett, T. Lindström, M. Oxborrow, Y. Harada, Y. Sekine, P. Meeson, and A. Y. Tzalenchuk, "Slow noise processes in superconducting resonators," *Phys. Rev. B* **87**, 140501 (2013).
- ³⁰J. Burnett, L. Faoro, I. Wisby, V. L. Gurtovoi, A. V. Chernykh, G. M. Mikhailov, V. A. Tulin, R. Shaikhaidarov, V. Antonov, P. J. Meeson, A. Y. Tzalenchuk, and T. Lindström, "Evidence for interacting two-level systems from the 1/f noise of a superconducting resonator," *Nature Communications* **5**, 4119 (2014).
- ³¹R. Barends, *Photon-detecting superconducting resonators*, Ph.D. thesis, Technische Universiteit Delft (2009).
- ³²S. Kumar, J. Gao, J. Zmuidzinas, B. A. Mazin, H. G. LeDuc, and P. K. Day, "Temperature dependence of the frequency and noise of superconducting coplanar waveguide resonators," *Applied Physics Letters* **92**, 123503 (2008), <https://doi.org/10.1063/1.2894584>.
- ³³A. N. Ramanayaka, B. Sarabi, and K. D. Osborn, "Evidence for universal relationship between the measured 1/f permittivity noise and loss tangent created by tunneling atoms," (2015), arXiv:1507.06043 [cond-mat.supr-con].
- ³⁴H. G. Leduc, B. Bumble, P. K. Day, B. H. Eom, J. Gao, S. Golwala, B. A. Mazin, S. McHugh, A. Merrill, D. C. Moore, O. Noroozian, A. D. Turner, and J. Zmuidzinas, "Titanium nitride films for ultrasensitive microresonator detectors," *Applied Physics Letters* **97**, 102509 (2010), <https://doi.org/10.1063/1.3480420>.
- ³⁵R. Barends, N. Vercruyssen, A. Endo, P. J. de Visser, T. Zijlstra, T. M. Klapwijk, and J. J. A. Baselmans, "Reduced frequency noise in superconducting resonators," *Applied Physics Letters* **97**, 033507 (2010), https://pubs.aip.org/aip/apl/article-pdf/doi/10.1063/1.3467052/14436926/033507_1_online.pdf.
- ³⁶S. R. Golwala, A. D. Beyer, D. Cunnane, P. K. Day, F. Defrance, C. F. Frez, X. Huang, J. Kim, J.-M. Martin, J. Sayers, S. Shu, and S. Yu, "NEW-MUSIC: The Next-generation Extended-Wavelength Multi-band Sub/millimeter Inductance Camera," in *Society of Photo-Optical Instrumentation Engineers (SPIE) Conference Series*, Society of Photo-Optical Instrumentation Engineers (SPIE) Conference Series, Vol. 13102, edited by J. Zmuidzinas and J.-R. Gao (SPIE, Bellingham, WA, 2024) pp. 1310202/1–42.
- ³⁷A. Kovács, P. S. Barry, C. M. Bradford, G. Chattopadhyay, P. Day, S. Doyle, S. Hailey-Dunsheath, M. Hollister, C. McKenney, H. G. LeDuc, N. Llombart, D. P. Marrone, P. Mauskopf, R. C. O'Brient, S. Padin, L. J. Swenson, and J. Zmuidzinas, "SuperSpec: design concept and circuit simulations," in *Society of Photo-Optical Instrumentation Engineers (SPIE) Conference Series*, Vol. 8452 (SPIE, Bellingham, Washington, 2012) pp. 84522G/1–10, astro-ph/1211.0934.